Macromolecular Materials and Engineering

www.mame-journal.de

RESEARCH ARTICLE OPEN ACCESS

Characterization of Copper- and Bronze-Filled PLA: Mechanical, Structural, and Biological Insights for Biomedical 3D and 4D Printing

Kinga Kardos[1,2] | Emese Paari-Molnar[1,2] | Roland Told[1,2] | Adel Len[3,4] | Peter Szabo[5,6] | Zoltan Ujfalusi[7] | Alexandra Steinerbrunner-Nagy[8] | Judit E. Pongracz[8] | Peter Maroti[1,2]

[1]3D Printing and Visualization Centre, University of Pecs, Pecs, Hungary | [2]Medical Skills Education and Innovation Centre, Medical School, University of Pecs, Pecs, Hungary | [3]Faculty of Engineering and Information Technology, University of Pécs, Pecs, Hungary | [4]HUN-REN Centre for Energy Research, Institute for Energy Security and Environmental Safety, Budapest Neutron Centre, Budapest, Hungary | [5]Institute of Geography and Earth Sciences, Faculty of Sciences, University of Pecs, Pecs, Hungary | [6]Environmental Analytical and Geoanalytical Research Group, Szentágothai Research Centre, University of Pecs, Pecs, Hungary | [7]Department of Biophysics, Medical School, University of Pecs, Pecs, Hungary | [8]Department of Pharmaceutical Biotechnology, Faculty of Pharmacy, University of Pecs, Pecs, Hungary

Correspondence: Emese Paari-Molnar (paari.molnar.emese@pte.hu)

Received: 4 August 2025 | **Revised:** 11 September 2025 | **Accepted:** 17 September 2025

Funding: This study was supported by the János Bolyai Research Scholarship of the Hungarian Academy of Sciences (Grant no. BO/00213/23).

Keywords: additive manufacturing | mechanical testing | polymer-metal composites | thermal analysis

ABSTRACT

Material extrusion (MEX), particularly Fused Filament Fabrication (FFF), is a widely used 3D printing technology, with growing interest in composite materials due to their broad range of applications. This study focuses on commercially available copper- and bronze-filled polylactic-acid (PLA) composites printed with FFF technology and on providing guidance for future practical applications, particularly in the biomedical field and 4D printing. In this research, static and dynamic mechanical tests, scanning electron microscopic imaging, and electric resistance measurements were conducted, and the thermal properties were determined by thermal conductivity measurements and differential scanning calorimetry, and thermogravimetric analysis (DSC-TGA). Cytotoxicity was assessed using an A549 cell viability assay. The results show that the material's brittleness increases in proportion to the volume percentage of metal particles; among the copper composites FormFutura MetalFil – Classic copper (29.14 vol.%) had the lower tensile strength (15.4 MPa ± 0.17 MPa), while for bronze composites, the tensile strength was lower for ColorFabb BronzeFill (33.64 vol.%, 17.7 MPa ± 0.54 MPa). Furthermore, these composites have no cytotoxic effect in short-term contact, and their enhanced thermal conductivity over traditional prosthetic materials makes them promising candidates for the development of prostheses intended to mitigate thermal discomfort.

1 | Introduction

Material extrusion (MEX) processes, like Fused Filament Fabrication (FFF), are among the most widely used 3D printing technologies [1, 2] processing thermoplastic polymers and composites by melting the filaments in an extruder and depositing the material layer-by-layer onto a plate that moves vertically [2, 3]. A wide selection of materials is available commercially, and research groups have also developed special, functional composites with enhanced mechanical, electrical, or biological properties [4, 5].

Additive manufacturing technologies have played a substantial role in the biomedical field, including advancements in diagnostics, intervention, and rehabilitation [6–8]. Previous research works widely explored the possibilities of 3D printing in education, communication between patients and healthcare providers, preoperative planning, medical device prototyping and development, as well as in prosthetics, orthotics, and implant manufacturing [9–15].

Numerous different fillers and matrix materials have been used in 3D printable composites, among which copper is particularly frequent due to its favorable physical characteristics, including excellent electric and thermal conductivity, and its remarkable resistance to corrosion in various environments [16, 17]. Furthermore, copper is noteworthy for its inherent antimicrobial properties, as it can inhibit the growth of microorganisms [18, 19]. The most well-known copper alloys are brass and bronze. Brass is more corrosionresistant and has better mechanical properties than pure copper, but because of the zinc content, it has decreased conductivity compared to pure copper. Bronze has significantly increased toughness and is also valued for its superior corrosion resistance and aesthetic appearance, which makes it suitable as a filler material [20, 21].

The integration of metal-filled PLA composites into 3D printing workflows opens potential avenues for 4D printing applications, particularly in the biomedical field [6]. The concept of 4D printing was first described by Skylar Tibbits in 2013, at a TED conference [22]. In this process, the 3D-printed materials can change their functionality, shape, and properties due to external stimuli like changes in humidity, temperature, level of light, or pH. Moreover, advanced 4D-printed structures can exhibit complex behaviors such as shape morphing, self-assembly, and self-repair, often triggered by electromagnetic fields or exposure to dynamic chemical or physical environments. These dynamic material responses open novel pathways in biomedical engineering, such as deployable stents, self-healing implants, or drug delivery systems that activate under specific physiological conditions [23–26].

Prior studies have explored custom-made and some commercially available PLA-copper and PLA-bronze composites, primarily focusing on 3D-printing parameters, with a limited examination of the mechanical properties of the composites. Kottasamy et al. developed copper-reinforced PLA filaments with 28 and 80 wt.% copper content and found that the samples with lower copper content exhibited more advantageous properties regarding mechanical parameters [16]. A study compared the mechanical properties and morphology of a PLA-copper composite to those of PLA and revealed that the presence of copper particles negatively affected the toughness of the material but improved the compression strength, dynamic linear elastic modulus, and hardening modulus [27].

A research group examined the influence of different infill patterns and densities on the FFF 3D-printed samples using commercially available copper composites (ColorFabb Copper Fill, Gizmo Dork Copper Metal Filled) [17]. Further research investigating the effect of infill pattern and density of the Gizmo Dork Copper Metal Filled filament compared to pure PLA showed that the tensile strength and elastic modulus of the copper composites were lower than those of the pure PLA for almost all the tested infill configurations [28]. The dimensional accuracy and porosity of the same ColorFabb material under different printing conditions were also investigated in another study, which proposed guidelines for the use of metal-filled filaments in the FFF process [29].

ColorFabb CopperFill and BronzeFill composites were also investigated by Vakharia et al., and the metal-reinforced PLA exhibited lower tensile strength and fracture toughness than pure PLA, regardless of the type of metal used as a filler [30].

A bronze-filled PLA composite was compared to pure PLA material in terms of mechanical properties, and it was found that both tensile strength and flexural strength of the pure material are greater than that of the bronze-PLA composite material [31]. A commercially available composite filament with 8% bronze content with PLA matrix material from eSun manufacturer was investigated, and the results of the study showed that the small amount of bronze in the composite changes the mechanical properties [32]. Moradi and his colleagues found that Kexcelled bronze-filled PLA exhibits poorer mechanical properties than pure PLA [33].

The thermal conductivity of the PLA is low, typically ranging from 0.09 to 0.25 W/(mK); however, the incorporation of metal fillers can enhance the thermal conductivity of the composite materials in comparison to pure polymer matrix [34–36]. A study examined the thermal properties of ColorFabb BronzeFill and CopperFill, finding that the composites did not exhibit the expected high thermal conductivity associated with metal particles that have a high weight percentage [37]. Materials with distinct thermal conductivity or glass transition behavior could be programmed to bend, contract, or expand when heated. Their tunable thermal and mechanical properties, combined with noncytotoxicity, position them as viable candidates for thermally responsive or shape-changing constructions [38]. These capabilities could be further explored to develop self-adaptive prosthetics, wearable electronics, or customized medical implants, where environmental responsiveness adds an additional layer of functionality [39]. Bronze- or copper-filled PLA might allow localized stiffness tuning or temperature-dependent movement, especially relevant in personalized assistive devices or wearables [40].

Although previous studies have examined copper and bronze as filler materials, most of these studies have focused on the effect of the printing parameters, and the available literature concerning the use of these composites remains limited. The aim of the present study is to evaluate the potential of commercially available copper- and bronze-filled PLA composite materials produced to be used with FFF technology in biomedical applications. To this end, the study provides a comprehensive investigation of the mechanical, structural, and biological properties of these materials, focuses on characteristics that are critical for the safe and reliable design of biomedical applications. Also, the research aimed to critically evaluate the selected copper- and bronze-filled filaments in order to provide informed guidance for future practical applications. A further objective is to assess the assumed thermal and electrical conductivity of these metal-filled composites, which supports their use in 4D-printing technologies that allow the development of structures that can respond to external stimuli.

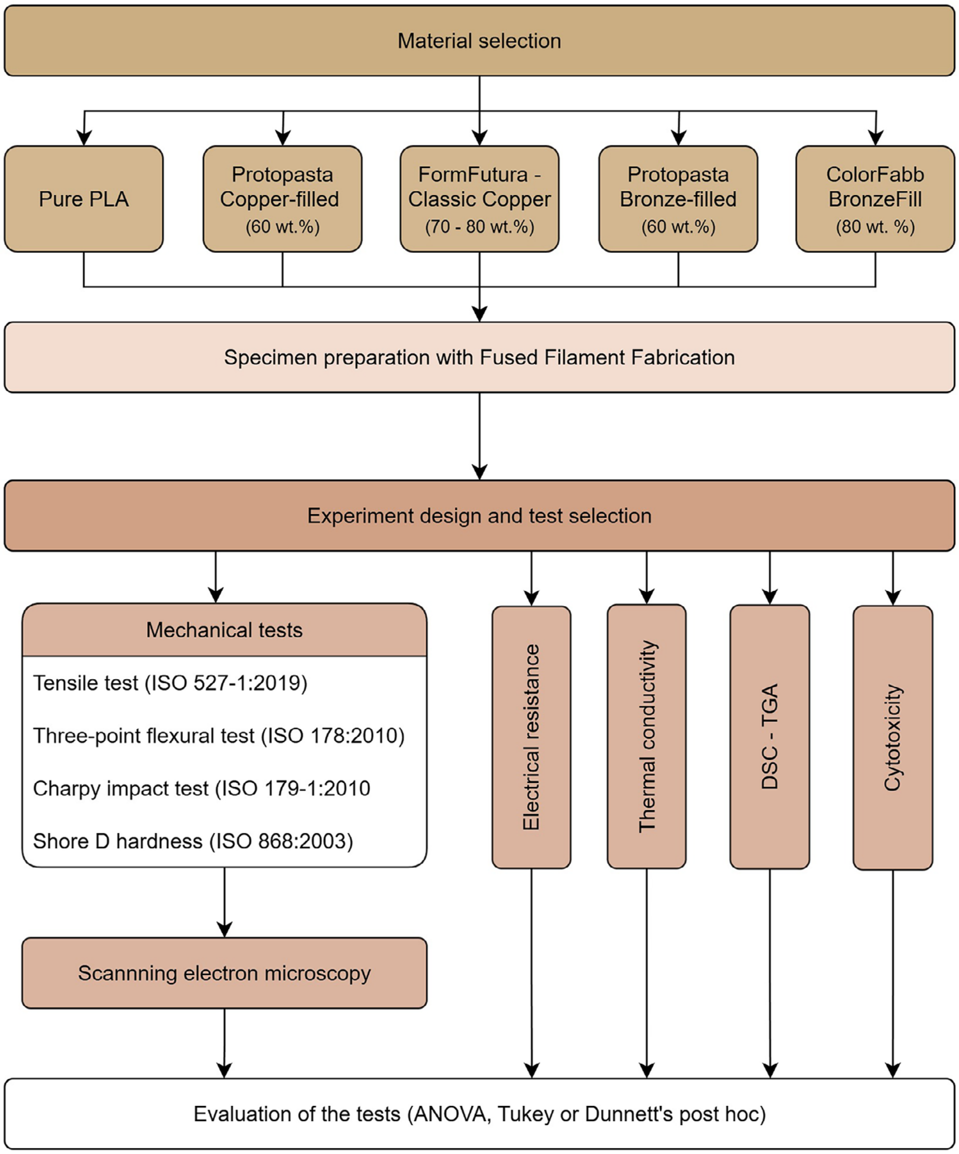

FIGURE 1 | Protocol of the study.

2 | Materials and Methods

This research was focused on PLA-based nonmagnetic metal composites, which do not require a sintering process and were developed for modeling, prototyping, and aesthetic purposes. The protocol of the study is illustrated in Figure 1.

2.1 | Test Materials and Specimen Preparation

Three manufacturers' PLA-metal composite filaments were subjected to examination and were compared to pure PLA filament (Herz Hungaria Ltd., Pesti rd. 284., Üllő 2225, Hungary) (Table 1). The BronzeFill Composite PLA was produced by ColorFabb (ColorFabb, Bremweg 7, 5951 DK Belfeld, The Netherlands). This PLA-based filament is loaded with bronze particles. The Bronze-Filled Metal Composite HTPLA and the Copper-Filled Metal Composite HTPLA were sourced from Protopasta (Protoplant Inc, 12001 NE 60th Way, Suite B-2, Vancouver, WA 98682), which are heat-treatable PLA-based filaments containing a high amount of metal powder. Additionally, the MetalFil – Classic Copper filament manufactured by FormFutura (Tarweweg 3, 6534 AM Nijmegen, The Netherlands) was also used. This PLA-based filament contains 80 wt.% copper filler.

The test specimens were produced by FFF technology, using a Craftbot+ 3D printer (Craftbot Ltd., Salgótarjáni rd. 12–14., Budapest 1087, Hungary), except for the MetalFil – Classic Copper, which was printed with an Ultimaker 3 Extended (Ultimaker B.V., Watermolenweg 24191 PN Geldermalsen, The Netherlands) due to the larger diameter of the filament. For materials printed with the Craftbot+ the filament diameter was 1.75 mm, the nozzle diameter was 600 μm, the extruder temperature was 210°C, and the heated bed temperature was 50°C. The specimens were printed with 200 μm layer height and 100% infill, and the printing speed was set to 30 mm/s. In the case of the material printed with the Ultimaker 3 Extended, the filament diameter was 2.85 mm. The extruder temperature was 220°C, the printing

TABLE 1 | Summary of commercially available metal-polymer composites used for specimen preparation.

Manufacturer	Official name of the filament	Abbreviated name of the material used in the article	Filament diameter (mm)
Herz Hungaria	PLA	PLA	1.75
Protopasta	Copper-Filled Metal Composite HTPLA	PP Copper	1.75
FormFutura	MetalFil – Classic Copper	FF Copper	2.85
Protopasta	Bronze-Filled Metal Composite HTPLA	PP Bronze	1.75
ColorFabb	BronzeFill Composite PLA	CF Bronze	1.75

speed was 50 mm/s, and all other printing parameters (nozzle, bed temperature, layer height, infill) were identical.

2.2 | Mechanical Tests

2.2.1 | Tensile Test

Tensile tests were conducted using a Zwick/Roell Z100 THW universal material tester (ZwickRoell, 89079, August-Nagel-Straße 11 Ulm, Germany) equipped with an extensometer. The measurements were carried out following the ISO 527-1:2019 standard, with A5 specimens (ISO 527-2:2012) [41]. The preload was set to 0.1 MPa, and the testing speed was 1 mm/min for the determination of tensile Young's modulus and then 2 mm/min for the rest of the test. The measurements were repeated five times at an ambient temperature (23°C ± 1°C) for every mechanical test. Photographs of the instruments and test specimens utilized during the testing processes are available in the Supporting Information.

2.2.2 | Three-Point Flexural Test

Three-point flexural tests were performed using the same Zwick/Roell Z100 THW universal material tester with preferred test specimens based on ISO 178:2019 standard [42]. The support distance was 64 mm. The tests were conducted with a preload of 0.1 MPa and at a consistent speed of 2 mm/min. The maximal strain was 4.7%.

2.2.3 | Charpy Impact Test

The impact values of the specimens were measured by a Zwick/Roell HIT50P (ZwickRoell, 89079, Ulm, Germany) instrument with a 5 J pendulum. The tests were performed in accordance with the ISO 179-1:2010 standard, on the edgewise of the test samples [43]. The dimensions of the specimens were 4 mm × 10 mm × 80 mm, without a notch.

2.2.4 | Shore D Hardness Measurement

Shore D hardness tests were conducted using a Zwick/Roell 3130/3131 instrument (ZwickRoell, 89079, August-Nagel-Straße 11 Ulm, Germany), which was placed on a stable stand during the measurement. The test was carried out according to ISO 868:2003 standard [44].

2.3 | Scanning Electron Microscopy

Scanning electron microscopy analyses were conducted on the fracture surface of the Charpy specimens with JEOL JSM-IT500HR SEM (3–1–2 Musashino, Akishima, Tokyo 196–8558, Japan) at 50x and 500x magnification. The samples were coated with gold using a JEOL JFC-1300 auto-fine coater.

2.4 | Electrical Resistance Measurement

Electrical resistance measurements were carried out using a Rohde & Schwarz HMC 8012 Digital Multimeter (Rohde & Schwarz GmbH & Co KG, Munich, Germany). Probes were positioned at equivalent locations on the surface of bolt nuts. The bolt nuts were then affixed to the endpoints of the specimens using screws.

2.5 | Thermal Conductivity Measurement

Thermal conductivity measurements were carried out on each of the investigated materials. The specimens were based on a disc with a diameter of 35 mm and a thickness of 5 mm. Figure 2 is a schematic representation of the measurement. The thermal conductivity factor of the materials was measured three times on three specimens of all investigated materials at temperatures 33°C, 37°C, and 40°C.

The measurement setup was controlled by an Arduino UNO (Arduino, Sommerville, MA, USA). Temperature was measured by two NTC temperature sensors on the opposite surfaces of the disc specimens. Heating was provided by a Rohde & Schwarz NGE100 Power Supply Series (Rohde & Schwarz GmbH & Co KG, Munich, Germany), which was controlled by a F~TEK SSR-10 DD Solid State Module (Techfun s. r. o., Žaškov, Slovak Republic). The power [W] was measured using a Rohde & Schwarz HMC 8012 Digital Multimeter (Rohde & Schwarz GmbH & Co KG, Munich, Germany). The heat flow ($\dot{Q}$[W]) can be calculated by deducting the heat loss from the measured power. The thermal conductivity was calculated by the following equation [11]:

$$\lambda = \left| \frac{\dot{Q}}{A \cdot \frac{T_2 - T_1}{\delta}} \right| \tag{1}$$

where λ [W/(mK)] is the thermal conductivity factor, $\dot{Q}$ [W] is the heat flow, A [m^2] is the cross section of the specimen, d [m] is the

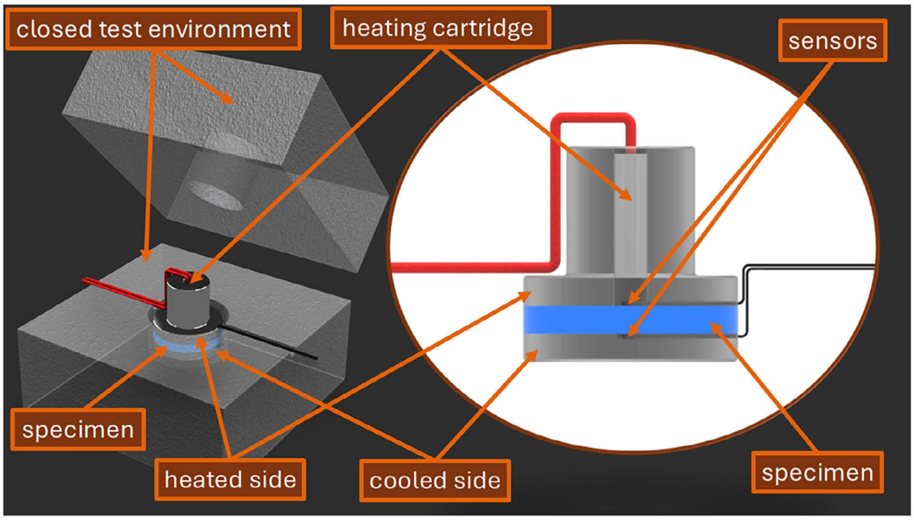

FIGURE 2 | Schematic representation of the thermal conductivity test.

distance between the two measurement points, and T_1, T_2 [K] are the measured temperatures at the surface of the specimen.

The zero-point correction factor (k) was calculated for each material using the ratio of the reference (from the literature) and the measured thermal conductivity factors ($\lambda_{\text{reference}}$, $\lambda_{\text{measured}}$) of a reference specimen from the investigated materials:

$$k = \frac{\lambda_{\text{reference}}}{\lambda_{\text{measured}}} \tag{2}$$

2.6 | Differential Scanning Calorimetry and Thermogravimetric Analysis (DSC-TGA)

The thermal properties of the investigated materials were analyzed using a LabSys Evo DSC-TGA (Setaram Ltd., 6 Rue de l'Oratoire, 69300 Calauire-et-Cuire, France) machine. The calibration of the temperature and enthalpy of the LabSys device was performed officially by the manufacturer. DSC-TGA measurements were performed under 100 mL/min nitrogen atmosphere, and the mass of each sample was set in the range from 8 to 13 mg. All measurements were carried in V = 100 µL uncovered Al_2O_3 crucibles (Setaram Ltd., 6 Rue de l'Oratoire, 69300 Calauire-et-Cuire, France) out up to 600°C with a heating rate of 10°C/min.

2.6.1 | Mass and Volume Ratio Calculations

For all metal-filled PLA composite materials, the proportion of metal in the material was estimated. In order to undertake this procedure, a 10 cm filament of each material was meticulously measured using an analytical balance (Ohaus Discovery DV215CD—Ohaus Corporation, 7 Campus Drive, Suite 310, Parsippany, NJ 07054, USA). This value was then calculated with due consideration for the average density of PLA and the filler. The mass ratio can be calculated in the following steps:

$$\rho_{\text{filament}} = \frac{m}{l \cdot d^2 \frac{\pi}{4}} \tag{3}$$

where ρ_{filament} is the density of the filament [g/cm^3], m is the measured mass of the filament [g], l is the length of the filament [cm], and d is the diameter of the filament [cm].

$$\frac{m_{\text{metal}}}{m} = 1 - \frac{\rho_{\text{PLA}}}{\rho} \cdot \frac{\rho - \rho_{\text{metal}}}{\rho_{\text{PLA}} - \rho_{\text{metal}}} \tag{4}$$

where m_{metal} is the mass of the metal part of the filament [g], m is the mass of the whole filament [g], ρ_{PLA} is the density of the PLA material [g/cm^3], ρ is the density of the filament [g/cm^3], and ρ_{metal} is the density of the metal in the filament [g/cm^3]. This calculation is based on average values found in the literature ($\rho_{\text{PLA,}}$ ρ_{metal}). To verify the calculation results, the reduction in mass during the TGA measurements was used as a metric.

To interpret the scanning electron microscopy results, the volume percentage of metal content in the tested materials was determined using the TGA results.

2.7 | Cytotoxicity Test

2.7.1 | Cell Cultures and Treatments

Human epithelial A549 cells (ATCC, Manassas, VA, Cat. No.: CRM-CCL-185) were cultured in Dulbecco's Modified Eagle Medium (DMEM; Lonza, Belgium, Cat. No.: 12604F) supplemented with 10% fetal bovine serum (FBS; Euroclone, Italy, Cat. No.: ECS0180L), 100 U/ml penicillin–streptomycin (Lonza, Belgium, Cat. No.: DE-17-602E), 0.1 mM nonessential amino acids (Lonza, Belgium, Cat. No.: 13-114E), 10 mM HEPES buffer (Lonza, Belgium, Cat. No.: 17-737E), and β-mercaptoethanol (Thermo Fisher Scientific, USA, MA, Cat. No.: 21985–023). Cells were maintained at 37°C in a humidified incubator with 5% CO_2.

A549 cells were suspended in DMEM and seeded into 24-well plates at a density of 3×10^4 cells per well in 1 mL of medium. Following an 8-h attachment period, 3D-printed polymer composite inserts were introduced into each well and co-cultured with the cells for 48 h under standard incubation conditions. Prior to cell exposure, the inserts were sterilized by UV irradiation (30 min per side, two rounds) to minimize the risk of contamination.

To establish a positive control for apoptosis, cells were treated with 1 μM staurosporine (Sigma–Aldrich, USA, Cat. No.: S-6942), a known inducer of programmed cell death. All viability experiments were performed in triplicate.

2.7.2 | Quantification of Cell Viability via Total Nucleic Acid Content

Cell viability was assessed based on total nucleic acid content using propidium iodide (PI) (Sigma–Aldrich, Cat. No.: 81845) staining, measured with a PerkinElmer EnSight multimode plate reader. This modified PI-based assay differs from conventional protocols by quantifying lysed cell-associated nucleic acids rather than selectively staining nonviable cells. After 48 h of incubation with the test materials, wells were rinsed with 500 μL phosphate-buffered saline (PBS, pH 7.4) to remove nonadherent apoptotic cells. Remaining adherent cells were lysed in 500 μL of alkaline borate buffer (pH 9.2) containing PI at a final concentration of 2 μg/mL.

After a 5-min incubation in the dark on an orbital shaker, fluorescence was measured at an excitation wavelength of 530 nm and emission at 620 nm. Data were normalized to untreated control wells to determine relative cell viability.

2.7.3 | Statistical Analysis

Statistical analyses and the graphical representations of the mechanical results were performed using OriginPro 2018 software (OriginLab Corporation, One Roundhouse Plaza, Northampton, MA, USA). After normality testing, the results of the measurements were compared using One Way ANOVA with Tukey post hoc test. The confidence interval was 95%. Power analyses were also carried out during the statistical tests, and the power level was above 0.98 in all cases.

The cell viability data were analyzed using GraphPad Prism 8.0. Normality was assessed using the Kolmogorov–Smirnov test. Statistical significance was determined using one-way ANOVA followed by Dunnett's post hoc test. Results were reported as significant at the following thresholds: $p < 0.0332$ (*), $p < 0.0021$ (**), $p < 0.0002$ (***), and $p < 0.0001$ (****).

3 | Results

3.1 | Mechanical Tests

3.1.1 | Tensile Test and Three-point Flexural Test

The results of the tensile and three-point flexural tests are presented together to facilitate a more comprehensive comparison of the main parameters.

The tensile Young's modulus of the pure PLA was 3373 MPa ± 82.1 MPa. Only one material exhibited no significant difference in this term: the FF MetalFil - Classic Copper, with a value of 3334 MPa ± 58.7 MPa, which was the lowest measured value. The other three materials had significantly higher Young's modulus, particularly the CF BronzeFill with 5547 MPa ± 155 MPa. The FF MetalFil - Classic Copper also exhibited significantly lower value in flexural Young's modulus than other materials, it was 2336 MPa ± 24.8 MPa. The highest flexural Young's modulus was observed in the case of the PP Copper-filled material, with 4682 MPa ± 53.8 MPa. Further results are presented in Figure 3.

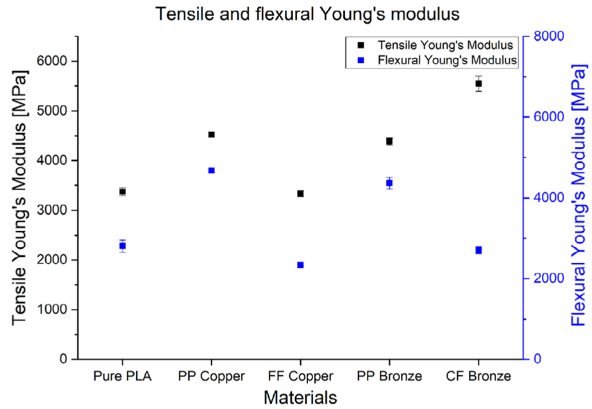

FIGURE 3 | Tensile and flexural Young's modulus of PLA and PLA-metal composites. The black squares indicate the tensile Young's modulus, while the blue squares refer to the flexural Young's modulus with standard deviations of the materials. Abbreviations: PP: Protopasta, FF: FormFutura, CF: ColorFabb.

The pure PLA exhibited the highest tensile strength and elongation at tensile strength, with a value of 52.13 MPa ± 1.33 MPa and 1.93% ± 0.01%, respectively. These values are significantly higher than those observed for other materials, with one exception in the elongation, which was similar for the PP Bronze-filled material as seen in Figure 4a. The lowest tensile strength and elongation at tensile strength were observed for the FF MetalFil - Classic Copper with 15.4 MPa ± 0.17 MPa and 0.93% ± 0.03%.

During the three-point flexural test, only the Pure PLA did not break until reaching the measured maximum deflection (4.7%). In addition to the pure PLA, the CF BronzeFill did not break until reaching the conventional deflection (3.5%). For these materials, only the stress at conventional deflection could be specified, which was 87.9 MPa ± 3.40 MPa for pure PLA and 41.9 MPa ± 2.64 MPa for the CF BronzeFill.

The highest flexural strength, which was measured for PP Bronze-Filled material, was 78.2 MPa ± 0.55 MPa, and the CF BronzeFill showed the highest strain at maximal flexural stress (3.06% ± 0.25%) as illustrated in Figure 4b. The lowest flexural strength was observed for the FF MetalFil - Classic Copper and strain at maximal flexural stress, 2336 MPa ± 24.8 MPa, 29.9 MPa ± 0.52 MPa, and 1.82% ± 0.12%, respectively.

3.1.2 | Charpy Impact Test

The Charpy impact strength was variable for the materials under examination, as illustrated in Figure 5. The highest

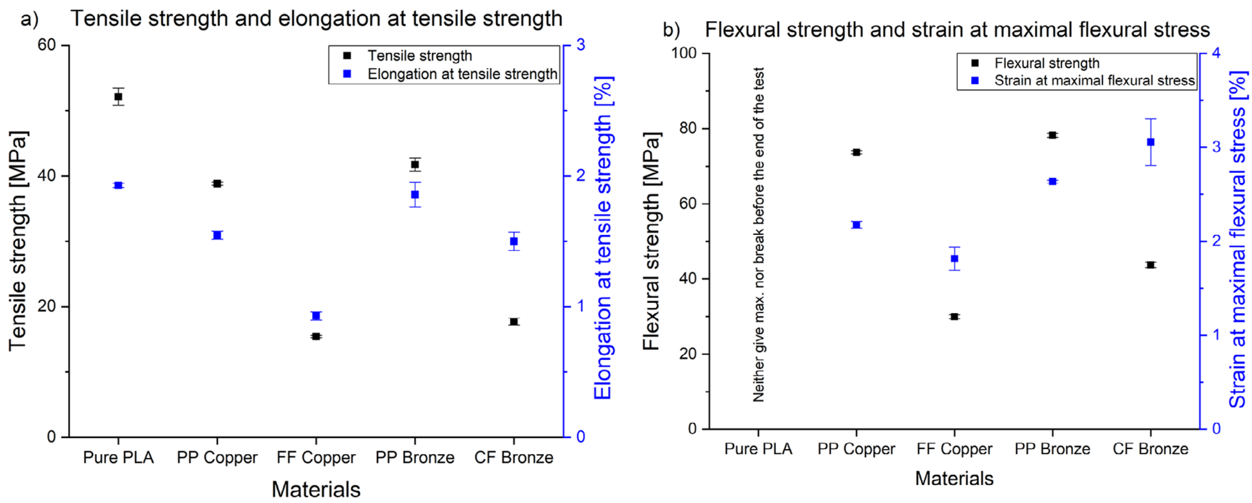

FIGURE 4 | Tensile and flexural properties of PLA and PLA-metal composites (a) Tensile strength (black squares) and elongation at tensile strength (blue squares) of examined materials, (b) Flexural strength (black squares) and strain at maximal flexural strength (blue squares) of the materials. Abbreviations: PP: Protopasta, FF: FormFutura, CF: ColorFabb.

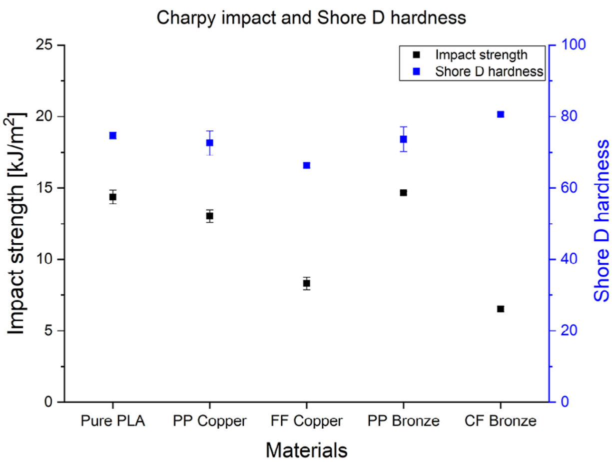

FIGURE 5 | Charpy impact strength and Shore D hardness of the PLA and PLA-metal composites. The black squares show the impact strength with standard deviation, while the blue squares indicate the Shore D hardness with corresponding standard deviations. Abbreviations: PP: Protopasta, FF: FormFutura, CF: ColorFabb.

impact strength was measured for the PP Bronze-filled material with a value of 14.65 kJ/m^2 $\pm$ 0.12 kJ/m^2, but the pure PLA (14.38 kJ/m^2 $\pm$ 0.47 kJ/m^2) and the other material from Protopasta (PP Copper-filled: 13.04 kJ/m^2 $\pm$ 0.43 kJ/m^2) exhibited similar values with no significant difference. The lowest impact strength was observed for the CF BronzeFill material, with 6.51 kJ/m^2 $\pm$ 0.20 kJ/m^2.

3.1.3 | Shore D Hardness

The hardness of the specimens made from CF BronzeFill was 80.5 $\pm$ 0.65, which was significantly higher than other materials. In contrast, the FF MetalFil - Classic Copper demonstrated the lowest Shore D hardness with a measured value of 66.3 $\pm$ 0.75. Figure 5 provides a detailed visual comparison of the measured hardness.

3.2 | Scanning Electron Microscopy

Scanning electron microscopy images were taken of the fracture surfaces of the Charpy specimens to gain insight into their internal structure. The SEM images revealed the presence of metal particles, but in varying forms within the composites. The original SEM images can be found in the supplementary materials in the SEM folder.

In the case of PP composites, the layer adhesion was poor, the printing layers were clearly separated, these can be seen in Figure 6a2 and a4. In these two materials, the metal particles exhibited an irregular shape and were found to adhere more strongly to the surrounding polymer matrix. The average metal particle size of the PP Copper-filled was 3–5 µm, whereas the PP Bronze-filled exhibited a wider range of particle sizes from 6 to 30 µm. Additionally, the number of visible particles was low, particularly in the PP Bronze-filled composite (Figure 6b2 and b4). The surface between the particles is observed to be smoother and having a structure similar to that of pure PLA.

The images of the FF MetalFil - Classic Copper and the CF BronzeFill demonstrate that the printing layers of these composites exhibited better adhesion compared to Protopasta composites. However, large pores can be observed (Figure 6a3 and a5). The distribution of spherical-shaped metal particles is mostly homogenous in both materials. The metal particles are clearly visible as separate from the polymer matrix, suggesting that their cohesion is poor (Figure 6b3 and b5). In these two materials, the diameter of the metal spheres demonstrate variability. It ranges from 5 to 25 µm for FF Copper, and from 10 to 25 µm for CF Bronze.

3.3 | Electrical Resistance Measurement

During the study, electrical resistance was found to be infinite in all cases of the metal composite materials that were analyzed. Consequently, it can be deduced that the materials examined do not facilitate the transmission of electricity.

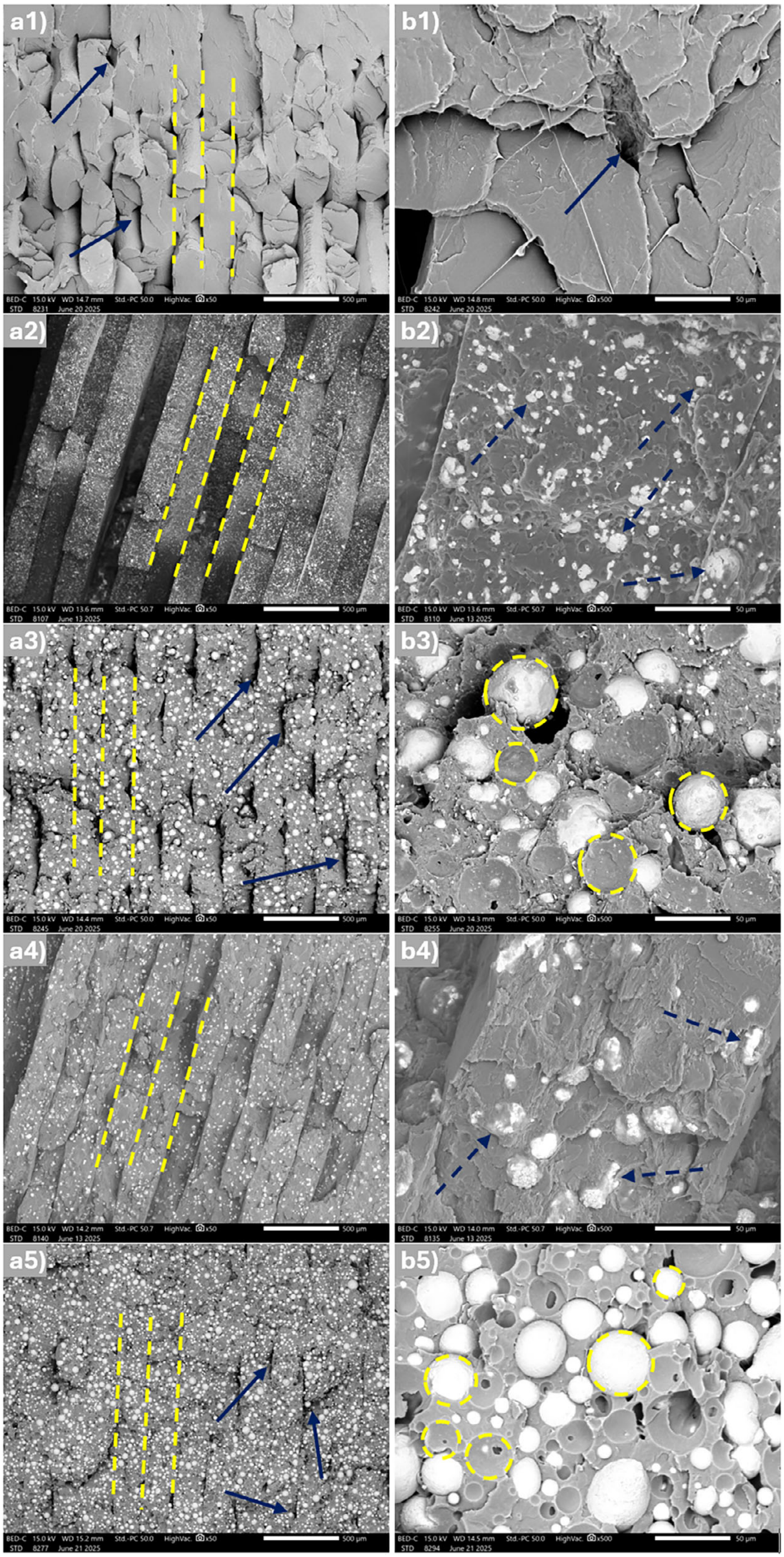

FIGURE 6 | The figure shows SEM images at two magnifications: (a) 50x and (b) 500x. Image 1) shows native PLA; 2) PP Copper; 3) FF Copper; 4) PP Bronze; and 5) CF Bronze. The marks represent the following: dashed lines indicate layer borders, blue arrows indicate gaps, dashed arrows indicate copper bronze particles, dashed circles indicate copper and bronze particles or their place. Abbreviations: PP: Protopasta, FF: FormFutura, CF: ColorFabb.

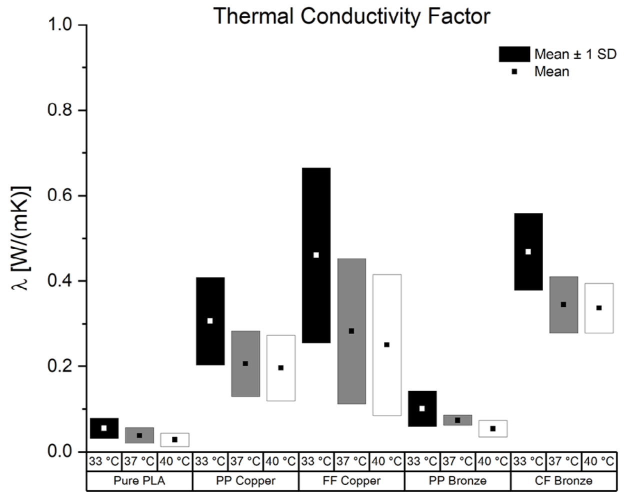

FIGURE 7 | Thermal conductivity factor of all investigated materials. The squares represent the mean of the measured values, while the size of the rectangles represents the standard deviation. Abbreviations: PP: Protopasta, FF: FormFutura, CF: ColorFabb.

3.4 | Thermal Conductivity

The thermal conductivity of all materials was investigated. As illustrated in Figure 7, the standard deviation of the thermal conductivity factor of specimens from materials from the manufacturer Protopasta (Bronze-filled and Copper-filled) is smaller than that of the other two metal-filled specimens. The thermal conductivity factor value of the two PP materials is also lower than (PP Copper: 0.21 W/(mK) ± 0.077 W/(mK), PP Bronze: 0.073 W/(mK) ± 0.012 W/(mK) at 37°C) that of the other two materials (FF Copper: 0.28 W/(mK) ± 0.17 W/(mK), CF Bronze: 0.34 W/(mK) ± 0.066 W/(mK)), but higher than that of Pure PLA material (0.038 W/(mK) ± 0.018 W/(mK) at 37°C).

3.5 | Differential Scanning Calorimetry and Thermogravimetric Analysis (DSC-TGA)

The materials have been tested with DSC-TG to validate the thermal conductivity results and to check the stability of the materials in the relevant temperature range. The parameters of the glass transition and the melting point temperatures are shown in Table 2.

3.6 | Mass Ratio Calculations

Density calculation was performed on all materials that were the subject of the investigation. For all metal-filled materials, TGA measurement was carried out and a calculation was conducted also to determine the mass ratio of the metal part of the composite. Table 3 represents the density (ρ) and mass ratio data (m_{metal}/m) from the manufacturer of the materials, calculated density of the materials (ρ_{CAL}), the measured and calculated metal mass ratio of composite materials (m_{metal}/m (TGA), m_{metal}/m (CAL)), and the deviation from the manufacturer's data ($\Delta(m/m)_{TGA}$, $\Delta(m/m)_{CAL}$, $\Delta(\rho)$).

TABLE 2 | Results of glass transition interval and melting points. T_{on} indicates the start of the glass transition intervals, T_g indicates the glass temperatures, T_{end} indicates the end of the glass intervals, and T_m indicates the melting points. FF copper and CF bronze particles or their place. Abbreviations: PP: Protopasta, FF: FormFutura, CF: ColorFabb.

Material	T_{on} (°C)	SD	T_g (°C)	SD	T_{end} (°C)	SD	T_m (°C)	SD
Pure PLA	64.63	0.86	66.66	0.48	69.64	0.62	155.2	0.75
PP copper	66.53	0.47	68.19	0.42	70.55	0.66	175.1	1.01
FF copper	58.97	0.76	60.79	0.48	63.00	0.30	152.2	0.04
PP bronze	66.23	0.40	67.79	0.53	70.34	1.17	177.8	0.84
CF bronze	57.13	0.50	59.25	0.11	61.98	0.51	154.7	0.41

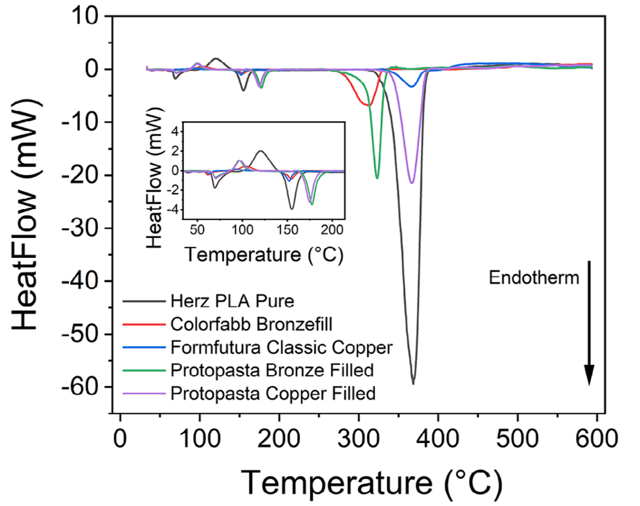

FIGURE 8 | Heating curves (30°C and 600°C) with melting peaks for all materials investigated. The curves represent the average of three measurements for each material. Inset: glass-transition-crystallization-melting phases.

The volume ratio for the metal composites was also calculated based on the results of the TGA measurements (Table 4).

Figure 8 represents the heating curves of the investigated materials. Similarly to the melting peaks (endotherm peaks between 150°C and 180°C in Figure 8), there is a decent shift for the crystallization (exotherm peaks in Figure 8) and glass phases (first endotherms between 60°C and 80°C in Figure 8) of the samples. The decomposition peaks (endotherm phases between 300°C and 400°C in Figure 8) also show some significant shift in peak-temperatures, it seems the bronze-containing samples start pyrolysis at a lower temperature. None of the above-mentioned thermal shifts affects the usability and other important mechanical properties of the samples. Furthermore, enthalpies were calculated and are shown in Table 5.

3.7 | Cytotoxicity

Cell viability assays revealed no statistically significant differences in cytotoxicity among the tested 3D-printed polymer

TABLE 3 | The data has been collected: density and mass ratio data from the manufacturer, TGA measurement data, and calculation data. The data will then be compared. Abbreviations: PP: Protopasta, FF: FormFutura, CF: ColorFabb.

Material	Manufacturer's data		Calculated and measured data			Deviation from manufacturer's data		
	ρ (g/cm^3)	m_{metal}/m (%)	ρ_{CAL} (g/cm^3)	m_{metal}/m (TGA) (%)	m_{metal}/m (CAL) (%)	$\Delta(m/m)_{TGA}$ (%)	$\Delta(m/m)_{CAL}$ (%)	$\Delta(\rho)$ (%)
Pure PLA	1.24	0	1.22	0	0	0	0	1.30
PP copper	2.3	60	2.33	61.6	54.91	2.67	8.49	1.18
FF copper	3.4	70-80	3.41	76.5	74.29	4.38	7.14	0.39
PP bronze	2.3	60	2.43	58.5	57.90	2.5	3.50	5.7
CF bronze	3.9	roughly 80	3.64	79.5	77.38	0.63	3.28	6.69

TABLE 4 | Measured V/V % for the metal composites. Abbreviations: PP: Protopasta, FF: FormFutura, CF: ColorFabb.

Material	V_{metal}/V (TGA) (%)
PP copper	16
FF copper	29.14
PP bronze	16.54
CF bronze	33.64

composite inserts. Following 48-h co-culture with A549 cells, the total nucleic acid content—used as a proxy for viable cell number—remained comparable across all treatment groups and did not significantly deviate from the untreated control. Fluorescence intensity values obtained from propidium iodide staining showed minimal variation, indicating that none of the composite materials induced measurable cell death or inhibited proliferation under the experimental conditions (Figure 9).

Positive control samples treated with 1 μM staurosporine exhibited a marked reduction in total nucleic acid content, confirming the assay's sensitivity to apoptotic cell death and validating the experimental setup. In contrast, all experimental inserts, regardless of their metallic filler content or polymer matrix composition, maintained high levels of cell viability.

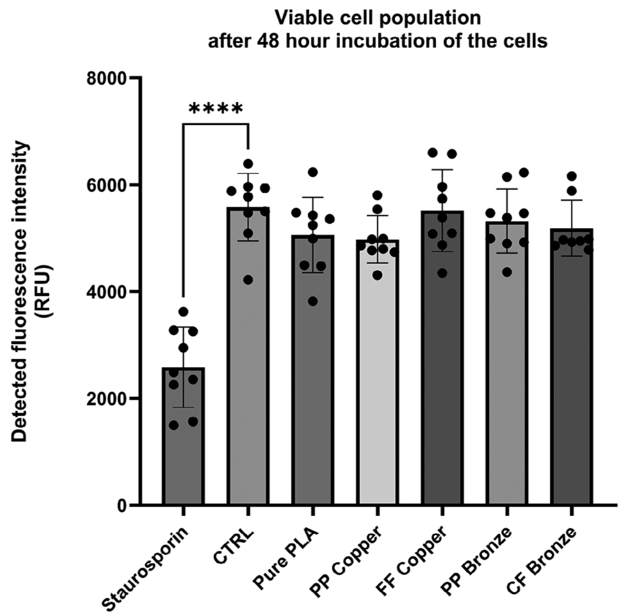

FIGURE 9 | Quantification of the living cell number after 48 h incubation of A549 cells in the presence of various 3D-printed metal-containing insets. The individual values measured are indicated by black dots. The significance levels were labelled according to the following: $p < 0.0001$ (****), nonsignificant differences are shown without asterisks. Abbreviations: PP: Protopasta, FF: FormFutura, CF: ColorFabb.

4 | Discussion

The utilization of composite materials in 3D printing is gaining popularity across a broad spectrum of applications, which leads to an increasing significance of research in this field. This study investigated commercially available metal-polymer composites focused on biomedical applications and the potential of 4D printing.

The addition of metal particles significantly alters the mechanical properties. The composites exhibited higher tensile Young's modulus, lower tensile strength, and elongation in comparison to pure PLA. These indicate an increase in the stiffness and brittleness of the material, resulting in enhanced susceptibility to fracture. This finding is consistent with the study by Vakharia et al., which includes the same CF BronzeFill composite that exhibited an elastic modulus of 5401 MPa and a tensile strength of 17 MPa [30]. Dal Maso and Cosmi also investigated this material and measured a tensile strength of 16.4 MPa ± 1.6 MPa [45]. These values are comparable to the 5547 MPa ± 155 MPa and 17.7 MPa ± 0.54 MPa measured by our research group.

PLA-bronze composites that have been investigated exhibit higher Shore D hardness than those containing copper, which is related to the quality of the filler. In comparison with data presented in another study, the Shore D hardness of a commercially available PLA-bronze composite was approximately 63, which is lower than that of the investigated bronze-containing materials (PP Bronze-filled: 73.6 ± 3.43, CF BronzeFill: 80.5 ± 0.65) [32].

Based on the Charpy impact test, the presence of metal particles does not necessarily result in a significant change in the impact

TABLE 5 | Enthalpy change values of the characteristic DSC peaks in the heating cycle of the different samples. The errors are standard deviations from at least three independent measurements.

	ΔH peak enthalpies (J/g) – heating (30–600°C)			
Materials	**Peak 1 Endotherm**	**Peak 2 Exotherm**	**Peak 3 Endotherm**	**Peak 4 Endotherm**
Pure PLA	9.71 ± 1.29	-19.47 ± 1.64	22.91 ± 0.58	798.21 ± 67.89
PP copper	4.64 ± 0.30	-6.65 ± 0.32	17.25 ± 1.40	262.64 ± 47.60
FF copper	1.19 ± 0.26	-1.28 ± 0.28	5.59 ± 0.50	48.17 ± 34.02
PP bronze	4.53 ± 1.26	-7.00 ± 1.32	21.64 ± 0.74	200.36 ± 12.65
CF bronze	2.08 ± 0.26	-3.86 ± 0.74	4.60 ± 0.21	107.13 ± 0.94

resistance of the material. Protopasta Copper- and Bronze-filled composites demonstrated similar values to pure PLA, whereas the FF MetalFil - Classic Copper and the CF BronzeFill had an impact strength less than two-thirds that of pure PLA. This is presumably related to the structure of the material, as demonstrated by the SEM images; the fillers in Protopasta Copper- and Bronze-filled materials are smaller and adhere more to the polymer matrix than in the case of the other two materials.

Taking the SEM images into account, it can be seen that the size of the filler particles varies greatly. In CF BronzeFill, the size of the particles ranges from 10 to 25 µm. This result corresponds to the results of Tedla and Rogers, who also reported heterogeneity in particle size in the same BronzeFill material [46]. In the case of the FF MetalFil - Classic Copper, the particle size varies from 5 to 25 µm, which contradicts the values measured by Alam and coworkers (75–100 µm) [47].

The TGA measurement was utilized to determine the metal mass and volume ratio. The volumetric metal content was consistent with the mechanical tests, indicating that materials with higher percentages of metal particles exhibited poorer mechanical strength, as confirmed by tensile, flexural, and Charpy impact tests. The findings of this study (79.5 wt.%) demonstrate similar values that the literature concerning the CF BronzeFill material (80.35 wt.%) [30]. The DSC signals of the samples provided the typical peaks for PLA samples, and the ratio between the enthalpies of the peaks is relatively the same for all tested samples.

The results of the cell viability test suggest that the tested metal-filled filaments are noncytotoxic to A549 epithelial cells in vitro, supporting their potential for safe application in biomedical and other biologically integrated technologies. This suggests short-term contact with the body (e.g., skin, mucosa) may be safe. However, it should be noted that the incubation period was only 48 h, and results are not guaranteed for longer periods of exposure to moist media. Bronze and copper fillers give the prints a metallic appearance and texture. The appearance mimics metal while maintaining PLA's safety and printability—useful for patient engagement and device personalization in case of production of assistive grips, sensory learning tools or rehabilitation objects, tools for pediatric or elderly patients.

Interestingly, despite being filled with conductive metal particles, the materials tested were found to be non-conductive and thus unsuitable for use as circuit components. The underlying cause of this phenomenon may be attributed to the uneven distribution of metal granules, the presence of alternating particle sizes, the low weight percentage of metal in the materials, or a combination of these factors. It is a worthwhile exercise to consider the potential for composites tested in this study to be used in combination with carbon-filled polymers, which are conductive in sensor technology in the future [13].

In this study, four composites containing metal particles with PLA matrix material and pure PLA were investigated. Mechanical properties, thermal conductivity, cytotoxicity and DSC/TGA measurements were carried out for each material. It can be hypothesized that, given the thermal conductivity of the CF BronzeFill and FF MetalFil - Classic Copper composite materials tested was within the range of human skin temperature, these metal-filled materials may be a suitable option for use in prosthetic casing or orthosis development. The measured thermal conductivity values are higher than the mentioned values in the literature [48–50]. This would result in a reduction in the discomfort and sweating experienced by the prosthesis or orthosis wearers due to heat [51].

As a future 4D application, these composites can be potentially used to create orthotic devices that gradually adjust their stiffness, offering enhanced support and personalized alignment during rehabilitation. Also, integration of metal fillers enhances thermal conductivity, enabling the fabrication of wearable sensors that can respond to body temperature changes or external heat to trigger further mechanical or functional transformations.

The paper's limitations can be attributed to the restricted range of materials that were examined. Materials from FormFutura, including a bronze-containing composite, and from ColorFabb, including a material containing copper particles, are available with the same matrix material as the materials investigated. It is acknowledged that alternative base materials could be selected for composites such as acrylonitrile butadiene styrene. However, the trend in biomedical applications is the use of PLA as a matrix material. The cell viability test could be complemented with a longer incubation period.

5 | Conclusion

The investigation of metal-filled polymer composites is ongoing, with the objective of understanding their properties and potential applications. This study investigated four metal-filled PLA composites and compared them to pure PLA. Two of the composites are filled with copper, while the remaining two are filled with bronze. The aim is to ascertain whether the composite materials could be used in biomedical applications and 4D-printing processes.

The outcomes of the mechanical experiments show that the composite materials are stiffer and more brittle than the pure PLA material. TGA measurements showed that the fillers increased stiffness. This is in line with the findings of the mechanical tests, which showed that results of lower magnitude were measured for higher percentages.

The investigated copper- and bronze-filled composites have no cytotoxic effect in short-term contact, suggesting their potential in biomedical use, especially in short-term contact devices on skin or mucosa.

The materials did not show any electrical conductivity, which would be expected with conductive fillers.

Thermal conductivity properties of the materials tested are superior to or equal to those of commercially available prosthetic coverings, making them suitable for orthoses and prostheses with the purpose of reducing perspiration and thereby rendering them more comfortable to wear.

Based on the mechanical, structural and biological tests performed, it has been determined that the materials under consideration are potential candidates for future 4D applications, mainly in the field of smart orthotics and external prosthetics, due to their favorable thermal properties.

Author Contributions

K.K. performed data curation, formal analysis, investigation, methodology, software, visualization, and writing – original draft. E.P.-M. performed data curation, formal analysis, investigation, methodology, software, visualization, and writing – original draft. R.T. performed conceptualization, investigation, methodology, software, validation, and writing – review and editing. A.L. performed data curation and investigation. P.S. acquired resources and performed investigation. Z.U. performed data curation, investigation, and writing – review and editing. A.S.-N. performed investigation, visualization, and writing – original draft. J.E.P. performed resources and writing – review and editing. P.M. performed conceptualization, funding acquisition, project administration, resources, supervision, and writing – review and editing.

Acknowledgements

The research team would like to express their thankfulness to the University of Pecs Medical School, and the University of Pecs 3D Printing and Visualization Centre. We sincerely appreciate the support of the János Bolyai Research Fellowship from the Hungarian Academy of Sciences awarded to Peter Maroti (BO/00213/23).

Conflicts of Interest

The authors declare no conflicts of interest.

Data Availability Statement

The data that support the findings of this study are openly available in Characterization of Copper- and Bronze-Filled PLA: Mechanical, Structural, and Biological Insights for Biomedical 3D and 4D Printing at https://doi.org/10.17632/2yn7dyjymk.2, reference number 0.

References

1. K. Rajan, M. Samykano, K. Kadirgama, W. S. W. Harun, and M. M. Rahman, "Fused Deposition Modeling: Process, Materials, Parameters, Properties, and Applications," *International Journal of Advanced Design and Manufacturing Technology* 120 (2022): 3–4.

2. International Organization for Standardization. ISO/ASTM 52900:2021 Additive manufacturing—General principles—Fundamentals and vocabulary, cited Oct 06, 2025, https://www.iso.org/standard/74514.html.

3. A. M. Lea, K. Matalgah, A. Yudhanto, and T. J. Fleck, "Effect of Thermal History on the Fracture and Fatigue Behaviors of Semi-Crystalline Polymers Prepared Via Material Extrusion Additive Manufacturing," *Materials and Design* 254, (2025): 114012, https://doi.org/10.1016/j.matdes.2025.114012.

4. M. Nikzad, S. H. Masood, and I. Sbarski, "Thermo-Mechanical Properties of a Highly Filled Polymeric Composites for Fused Deposition Modeling," *Materials and Design* 32, no. 6 (2011): 3448–3456, https://doi.org/10.1016/j.matdes.2011.01.056.

5. P. Musto, P. L. Manna, F. Cimino, G. Mensitieri, and P. Russo, "Morphology, Molecular Interactions and H2O Diffusion in a Poly(Lactic-Acid)/Graphene Composite: A Vibrational Spectroscopy Study," *Spectrochimca Acta Part A Molecular and Biomolecular Spectroscopy* 218, (2019) 40, https://doi.org/10.1016/j.saa.2018.08.019.

6. I. Buj-Corral, H. Sanz-Fraile, A. Ulldemolins, et al., "Characterization of 3D Printed Metal-PLA Composite Scaffolds for Biomedical Applications," *Polymers* 14, (2022): 2754, https://doi.org/10.3390/polym14132754.

7. Á. T. Schlégl, R. Told, K. Kardos, A. Szőke, Z. Ujfalusi, and P. Maróti, "Evaluation and Comparison of Traditional Plaster and Fiberglass Casts With 3D-Printed PLA and PLA–CaCO3 Composite Splints for Bone-Fracture Management," *Polymers* 14, no. 17 (2022): 3571, https://doi.org/10.3390/polym14173571.

8. P. Maróti, P. Varga, A. Ferencz, Z. Ujfalusi, M. Nyitrai, and D. Lőrinczy, "Testing of Innovative Materials for Medical Additive Manufacturing by DTA," *Journal of Thermal Analysis and Calorimetry* 136, (2019): 2041–2048, https://doi.org/10.1007/s10973-018-7839-x.

9. J. Szalma, B. V. Lovász, E. Lempel, and P. Maróti, "Three-Dimensionally Printed Individual Drill Sleeve for Depth-Controlled Sections in Third Molar Surgery," *Journal of Oral and Maxillofacial Surgery* 77, no. 4 (2019): 704.e1–704.e7, https://doi.org/10.1016/j.joms.2018.11.028.

10. K. Kardos, R. Told, A. Pentek, N. Sahai, K. Banfai, and A. Vizi, "Surface Disinfection Change the Mechanical, Structural and Biological Properties of Flexible Materials Used for Additive Manufacturing of Medical Devices," *Materials and Design* 237, (2024): 112616, https://doi.org/10.1016/j.matdes.2023.112616.

11. L. Kelava, I. Ivic, E. Pakai, et al., "Stereolithography 3D Printing of a Heat Exchanger for Advanced Temperature Control in Wire Myography," *Polymers* 14, no. 3 (2022): 471, https://doi.org/10.3390/polym14030471 .

12. S. Rendeki, B. Nagy, M. Bene, et al., "An Overview on Personal Protective Equipment (PPE) Fabricated With Additive Manufacturing Technologies in the Era of COVID-19 Pandemic," *Polymers* 12, (2022):2703, https://doi.org/10.3390/polym12112703.

13. E. Paari-Molnar, K. Kardos, R. Told, et al., "Comprehensive Study of Mechanical, Electrical and Biological Properties of Conductive Polymer Composites for Medical Applications Through Additive Manufacturing," *Polymers* 16, no. 18 (2024): 2625, https://doi.org/10.3390/polym16182625.

14. Z. Ujfalusi, A. Pentek, R. Told, A. Schiffer, M. Nyitrai, and P. Maroti, "Detailed Thermal Characterization of Acrylonitrile Butadiene Styrene and Polylactic Acid Based Carbon Composites Used in Additive Manufacturing," *Polymers* 12, no. 12 (2020): 2960, https://doi.org/10.3390/polym12122960.

15. A. Moghanian, P. Asadi, M. Akbari, et al., "New Trends in 3D and 4D Printed Dental and Orthopedic Implants: Methods, Applications and Future Directions," *Bioprinting* 48, (2025): 00406, https://doi.org/10.1016/j.bprint.2025.e00406.

16. A. Kottasamy, M. Samykano, K. Kadirgama, M. Rahman, and M. M. Noor, "Experimental Investigation and Prediction Model for Mechanical Properties of Copper-Reinforced Polylactic acid Composites (Cu-PLA) Using FDM-Based 3D Printing Technique," *International Journal of Advanced Manufacturing Technology* 119, (2022): 5211, https://doi.org/10.1007/s00170-021-08289-4.

17. M. Hamoud, A. B. Elshalakany, M. Gamil, and H. Mohamed, "Investigating the Influence of 3D Printing Parameters on the Mechanical Characteristics of FDM Fabricated (PLA/Cu) Composite Material," *International Journal of Advanced Manufacturing Technology* 134, (2024): 3769, https://doi.org/10.1007/s00170-024-14313-0.

18. S. Ekonomou, S. Soe, and A. C. Stratakos, "An Explorative Study on the Antimicrobial Effects and Mechanical Properties of 3D Printed PLA and TPU Surfaces Loaded with Ag and Cu Against Nosocomial and Foodborne Pathogens," *Journal of Mechanical Behavior of Biomedical Materials* 137, (2023): 105536, https://doi.org/10.1016/j.jmbbm.2022.105536.

19. D. A. Montero, C. Arellano, M. Pardo, R. Vera, R. Gálvez, and M. Cifuentes, "Antimicrobial Properties of a Novel Copper-Based Composite Coating With Potential for Use in Healthcare Facilities," *Antimicrobial Resistance and Infection Control* 8, no. 3 (2019): 1, https://doi.org/10.1186/s13756-018-0456-4.

20. T. Dobson, N. Larrosa, M. Reid, K. Rajamudili, S. Ganguly, and H. Coules, "Corrosion Mechanisms of Plasma Welded Nickel Aluminium Bronze Immersed in Seawater," *Corrosion Science* 232, (2024): 112004, https://doi.org/10.1016/j.corsci.2024.112004.

21. M. Mousapour, S. S. Kumar, J. Partanen, and M. Salmi, "3D Printing of a Continuous Carbon Fiber Reinforced Bronze-Matrix Composite Using Material Extrusion," *Composites Part B Engineering* 289, (2025): 111961, https://doi.org/10.1016/j.compositesb.2024.111961.

22. S. Tibbits, The Emergence of "4D Printing" | TED Talk, https://www.ted.com/talks/skylar_tibbits_the_emergence_of_4d_printing/transcript.

23. S. Tibbits, "4D Printing: Multi-Material Shape Change," *Architectural Design* 84, (2014): 116, https://doi.org/10.1002/ad.1710.

24. F. Momeni, S. M. M. Hassani, X. Liu, and J. Ni, "A Review of 4D Printing," *Materials and Design* 122, (2017): 42, https://doi.org/10.1016/j.matdes.2017.02.068.

25. Z. X. Khoo, J. E. M. Teoh, Y. Liu, et al., "3D Printing of Smart Materials: A Review on Recent Progresses in 4D Printing," *Virtual and Physical Prototyping* 10, (2015): 103, https://doi.org/10.1080/17452759.2015.1097054.

26. H. Doostmohammadi, M. Baniassadi, M. Bodaghi, and M. Baghani, "4D Printing of Magneto-Thermo-Responsive PLA/PMMA/Fe3O4 Nanocomposites with Superior Shape Memory and Remote Actuation," *Macromolecular Materials and Engineering* 309, (2024): 2400090, https://doi.org/10.1002/mame.202400090.

27. Q. Ji, Z. Wang, J. Yi, and X. Tang, "Mechanical Properties and a Constitutive Model of 3D-Printed Copper Powder-Filled PLA Material," *Polymers* 13, (2021): 3605, https://doi.org/10.3390/polym13203605.

28. R. Kumaresan, A. Kottasamy, J. Mogan, et al., "Preliminary Investigation on the Tensile Properties of FDM Printed PLA/ Copper Composite," *Materials Today Proceedings* 109, (2023): 87–92, https://doi.org/10.1016/j.matpr.2023.10.054.

29. I. Buj-Corral and M. Sivatte-Adroer, "An Experimental Investigation about the Dimensional Accuracy and the Porosity of Copper-Filled PLA Fused Filament Fabrication Parts," *Metals* 13, (2023): 1608, https://doi.org/10.3390/met13091608.

30. V. S. Vakharia, L. Kuentz, A. Salem, et al., "Additive Manufacturing and Characterization of Metal Particulate Reinforced Polylactic Acid (PLA) Polymer Composites," *Polymers* 13, (2021): 3545, https://doi.org/10.3390/polym13203545.

31. E. D. Stolen, T. Wu, J. B. Schulz, et al.,"*IOP Conference Series of Materials Science Engineering* 376, (2018): 012042, https://iopscience.iop.org/article/10.1088/1757-899X/376/1/012042.

32. M. M. Hanon, Y. Alshammas, and L. Zsidai, "Effect of Print Orientation and Bronze Existence on Tribological and Mechanical Properties of 3D-Printed Bronze/PLA Composite," *International Journal of Advanced Manufacturing Technology* 108, (2020): 553–570, https://doi.org/10.1007/s00170-020-05391-x.

33. M. Moradi, M. K. Moghadam, M. Shamsborhan, and M. Bodaghi, "The Synergic Effects of FDM 3D Printing Parameters on Mechanical Behaviors of Bronze Poly Lactic Acid Composites," *Journal of Composites Science* 4, (2020): 17, https://doi.org/10.3390/jcs4010017.

34. S. Islam, G. Bhat, and P. Sikdar, "Thermal and Acoustic Performance Evaluation of 3D-Printable PLA Materials," *Journal of Building Engineering* 7, (2023): 105979, https://doi.org/10.1016/j.jobe.2023.105979.

35. N. Angin, S. Caylak, M. Ertas, and A. Donmez Cavdar, "Effect of Alkyl Ketene Dimer on Chemical and Thermal Properties of Polylactic Acid (PLA) Hybrid Composites," *Sustainable Materials and Technologies* 32, (2022): 00386, https://doi.org/10.1016/j.susmat.2021.e00386.

36. B. Almuallim, W. S. W. Harun, I. J. Al Rikabi, and H. A. Mohammed, "Thermally Conductive Polymer Nanocomposites for Filament-Based Additive Manufacturing," *Journal of Materials Science* 57, (2022): 3993–4019, https://doi.org/10.1007/s10853-021-06820-2.

37. J. Laureto, J. Tomasi, J. A. King, and J. M. Pearce, "Thermal Properties of 3D Printed Polylactic Acid-Metal Composites," *Progress in Additive Manufacturing* 2, (2017): 57–71, https://doi.org/10.1007/s40964-017-0019-x.

38. O. C. Abdol-Hamid, Y. Wang, S. Farzinazar, C. Yang, H. Lee, and J. Lee, "Tunable Thermal Transport in 4D Printed Mechanical Metamaterials," *Materials and Design* 231, (2023): 111992, https://doi.org/10.1016/j.matdes.2023.111992.

39. R. Pugliese and S. Regondi, "Artificial Intelligence-Empowered 3D and 4D Printing Technologies toward Smarter Biomedical Materials and Approaches," *Polymers* 14, no. 14 (2022): 2794, https://doi.org/10.3390/polym14142794.

40. S. Vennam, V. KN, and F. Pati, "3D Printed Personalized Assistive Devices: A Material, Technique, and Medical Condition Perspective," *Applied Materials Today* 40, (2024): 102403, https://doi.org/10.1016/j.apmt.2024.102403.

41. International Organization for Standardization ISO 527-1:2019 Plastics Determination of tensile properties Part 1: General principles. Ics 8308001, cited Oct 06, 2025, https://www.iso.org/standard/75824.html.

42. International Organization for Standardization, ISO 178:2019 Plastics Determination of flexural properties, cited Oct 06, 2025, https://www.iso.org/standard/70513.html.

43. ISO 179-1:2010 Plastics — Determination of Charpy impact properties — Part 1: Non-instrumented impact test, cited Oct 06, 2025, https://www.iso.org/standard/44852.html.

44. International Organization for Standardization, ISO 868:2003, cited Oct 06, 2025, https://www.iso.org/standard/34804.html.

45. A. Dal Maso and F. Cosmi, "Mechanical Characterization of 3D Printed Objects," *Materials Today Proceedings* 5, no. 13 (2018): 26739–26746, https://doi.org/10.1016/j.matpr.2018.08.145.

46. G. Tedla and K. Rogers, "Characterization of 3D Printing Filaments Containing Metal Additives and Their Particulate Emissions," *Science of the Total Environment* 875, (2025) 162648, https://doi.org/10.1016/j.scitotenv.2023.162648.

47. F. Alam, V. R. Shukla, K. M. Varadarajan, and S. Kumar, "Microarchitected 3D Printed Polylactic Acid (PLA) Nanocomposite Scaffolds

for Biomedical Applications," *Journal of Mechanical Behavior Biomedical Materials* 103, (2020): 103576, https://doi.org/10.1016/j.jmbbm.2019.103576.

48. S. A. Abbood, Z. Wu, and B. Sundén, "Theremal Assessment for Prostheses: State of the Art View," *International Journal of Computational Methods and Experimental Measurements* 5, no. 1 (2017): 1–12, https://doi.org/10.2495/CMEM-V5-N1-1-12.

49. C. M. Webber, M. R. Klittich, A. Dhinojwala, and B. L. Davis, "Thermal Conductivities of Commercially Available Prosthetic Materials," *Journal of Prosthetics and Orthotics* 26, no. 4 (2014):212–215, https://doi.org/10.1097/JPO.0000000000000043.

50. G. K. Klute, G. I. Rowe, A. V. Mamishev, and W. R. Ledoux, "The Thermal Conductivity Of Prosthetic Sockets and Liners," *Prosthetics and Orthotics International* 31, no. 3 (2007): 292–299, https://doi.org/10.1080/03093640601042554.

51. K. Ghoseiri and M. R. Safari, "Prevalence of Heat and Perspiration Discomfort Inside Prostheses: Literature Review," *Journal of Rehabilitation Research & Development* 51, no. 6 (2014): 855, https://doi.org/10.1682/JRRD.2013.06.0133.